Structural Comparison of Iron Tetrapolyvanadate $Fe_2V_4O_{13}$ and Iron Polyvanadomolybdate $Fe_2V_{3.16}Mo_{0.84}O_{13.42}$: A New Substitution Mechanism of Molybdenum(VI) for Vanadium(V)

Xiandong Wang, Kevin R. Heier, Charlotte L. Stern, and Kenneth R. Poeppelmeier*

Department of Chemistry, Northwestern University, Evanston, Illinois 60208-3113

Received August 7, 1998

Single crystals of the iron tetrapolyvanadate $Fe_2V_4O_{13}$ and the iron polyvanadomolybdate $Fe_2V_{3.16}Mo_{0.84}O_{13.42}$ were grown from Fe_2O_3/V_2O_5 and $Fe_2O_3/V_2O_5/MoO_3$ melts, respectively. Single-crystal X-ray diffraction revealed that the two structures are closely related. Both contained isolated Fe_2O_{10} octahedral dimers with similar orientations. The unusual *U*-shaped $V_4O_{13}^{6-}$ clusters in $Fe_2V_4O_{13}$ were ordered while the *U*-shaped $[V_{3.16}Mo_{0.84}O_{13.42}]^{6-}$ clusters in $Fe_2V_{3.16}Mo_{0.84}O_{13.42}$ were disordered. The substitution of molybdenum(VI) for vanadium(V) revealed a new substitution mechanism, in which a corresponding stoichiometric amount of oxygen was brought into the structure for charge balance with no reduction of the V^{5+} and Mo^{6+} ions. Crystal data: for $Fe_2V_4O_{13}$, monoclinic, space group $P2_1/c$ (No. 14), with $a = 8.300(2)$ Å, $b = 9.404(6)$ Å, $c = 14.560(2)$ Å, $\beta = 102.08(1)°$, and $Z = 4$; for $Fe_2V_{3.16}Mo_{0.84}O_{13.42}$, monoclinic, space group $P2_1/c$ (No. 14), with $a = 7.678(1)$ Å, $b = 9.456(2)$ Å, $c = 8.336(2)$ Å, $\beta = 109.50(2)°$, and $Z = 2$.

Introduction

Multicomponent vanadates/molybdates have been found to be effective catalysts for many catalytic reactions such as selective oxidation of hydrocarbons (P−V−O and V−Mo−O), selective reduction of NO_x (Ti−W−V−O), and ammoxidation of hydrocarbons (Sb−V−O and Fe−Bi−Mo−O). The active phases in these catalyst systems are usually binary or ternary compounds. For instance, $(VO)_2P_2O_7$ in the P−V−O system and $SbVO_4$ in the Sb−V−O system are the active phases for the oxidation of *n*-butane to maleic anhydride and ammoxidation of propene, respectively. The aim of the present research is to explore new and interesting vanadates/molybdates and to understand their remarkable solid-state chemistry. $MgO-V_2O_5-MoO_3$ is an interesting system in the search for alkane dehydrogenation catalysts. Binary compounds MgV_2O_6, $Mg_2V_2O_7$, $Mg_3V_2O_8$, and $MgMoO_4$ have shown activity for the oxidative dehydrogenation of propane to propene and butane to butenes.[1] Our previous study[2] on the $MgO-V_2O_5-MoO_3$ system revealed the ternary compound $Mg_{2.5}VMoO_8$, which showed good selectivity for the dehydrogenation of butane to butenes and butadiene.[3] Further investigation on the $MO-V_2O_5-MoO_3$ systems has established a series of solid solutions $M_{2.5+x}V_{1+2x}Mo_{1-2x}O_8$ ($M = Mg^{2+}$, Zn^{2+}, Mn^{2+}),[4] in which the oxygen content is constant and the change in charge from the V^{5+}/Mo^{6+} substitution is balanced by the concentration of divalent cations.

The $Fe_2O_3-V_2O_5-MoO_3$ system was selected to study the replacement of divalent metal oxides with trivalent metal oxides. This system was investigated about a decade ago, and $FeVMoO_7$, $Fe_4V_2Mo_3O_{20}$, and $Fe_2V_4O_{13}$ were reported.[5] However, no structural information was available until Permer and co-workers recently investigated them with powder X-ray diffraction.[6] Our single-crystal X-ray studies[7] confirmed their reported $FeVMoO_7$ and $Fe_4V_2Mo_3O_{20}$ structures. In this paper, the structures of $Fe_2V_4O_{13}$ and a new compound $Fe_2V_{3.16}Mo_{0.84}O_{13.42}$ have been investigated by single-crystal X-ray diffraction. A new substitution mechanism of Mo^{6+} for V^{5+} is proposed. During the preparation of this paper, Permer and Laligant reported the structure of $Fe_2V_4O_{13}$ determined by powder X-ray diffraction,[6a] which was consistent with our results reported below.

Experimental Section

Synthesis. $Fe_2V_4O_{13}$ crystals were grown by a flux method using a sealed-tube technique. A starting composition containing 5 mol % Fe_2O_3 (99.9%, Aldrich) and 95 mol % V_2O_5 (99.6+%, Aldrich) (composition A in Figure 1) was chosen within the very narrow crystallization zone of $Fe_2V_4O_{13}$ (93−97.5 mol % V_2O_5) in the $Fe_2O_3-V_2O_5$ phase diagram.[8] About 5 g of mixed powder was packed into a platinum boat and sealed in a quartz tube by a hydrogen−oxygen torch. The sample was heated to 700 °C and soaked for 2 h, then cooled to 600 °C at 4 °C h^{-1}, and

* Corresponding author (E-mail, krp@nwu.edu; Fax, (847) 491-7713).

(1) (a) Michalakos, P. M.; Kung, M. C.; Jahan, I.; Kung, H. H. *J. Catal.* **1993**, *140*, 226−242. (b) Owen, O. S.; Kung, H. H. *J. Mol. Catal.* **1993**, *79*, 265−284. (c) Soenen, V.; Herrmann, J. M.; Volta, J. C. *J. Catal.* **1996**, *159*, 410−417. (d) Lee, K. H.; Yoon, Y. S.; Ueda, W.; Moro-oka, Y. *Catal. Lett.* **1997**, *46*, 267−271. (e) Cadus, L. E.; Gomez, M. F.; Abello, M. C. *Catal. Lett.* **1997**, *43*, 229−233.

(2) Zubkov, V. G.; Leonidov, I. A.; Poeppelmeier, K. R.; Kozhevnikov, V. L. *J. Solid State Chem.* **1994**, *111*, 197−201.

(3) Harding, W. D.; Kung, H. H.; Kozhevnikov, V. L.; Poeppelmeier, K. R. *J. Catal.* **1993**, *144*, 597−610.

(4) (a) $Mg_{2.5}VMoO_8$: Wang, X. D.; Stern, C. L.; Poeppelmeier, K. R. *J. Alloys Compd.* **1996**, *243*, 51−58. (b) $Zn_{2.5}VMoO_8$: Wang, X. D.; Heier, K. R.; Stern, C. L.; Poeppelmeier, K. R. *J. Alloys Compd.* **1997**, *255*, 190−194. (c) $Mn_{2.5}VMoO_8$: Wang, X. D.; Heier, K. R.; Stern, C. L.; Poeppelmeier, K. R. *J. Alloys Compd.* **1998**, *267*, 79−85.

(5) (a) Kurzawa, M. *Thermochim. Acta* **1985**, *92*, 563−566. (b) Walczak, J.; Kurzawa, M.; Trzesniowska, L. *Thermochim. Acta* **1985**, *92*, 567−570. (c) Walczak, J.; Kurzawa, M.; Wasaznik, K. *Thermochim. Acta* **1985**, *92*, 571−574.

(6) (a) $Fe_2V_4O_{13}$: Permer, L.; Laligant, Y. *Eur. J. Solid State Inorg. Chem.* **1997**, *34*, 41−52. (b) $FeVMoO_7$: Lebail, A.; Permer, L.; Laligant, Y. *Eur. J. Solid State Inorg. Chem.* **1995**, *32*, 883−892. (c) $Fe_4V_2Mo_3O_{20}$: Laligant, Y.; Permer, L.; Lebail, A. *Eur. J. Solid State Inorg. Chem.* **1995**, *32*, 325−334.

(7) (a) $FeVMoO_7$: Wang, X. D.; Heier, K. R.; Stern, C. L.; Poeppelmeier, K. R. *Inorg. Chem.* **1998**, *37*, 3252−3256. (b) $Fe_4V_2Mo_3O_{20}$: Wang, X. D.; Stern, C. L.; Poeppelmeier, K. R. In preparation.

(8) Fotiev, A. A.; Cheshnitskii, S. M.; Surat, L. L. *Russ. J. Inorg. Chem. (Engl. Transl.)* **1983**, *28*, 560−562.

10.1021/ic980942t CCC: $15.00
Published on Web 12/05/1998

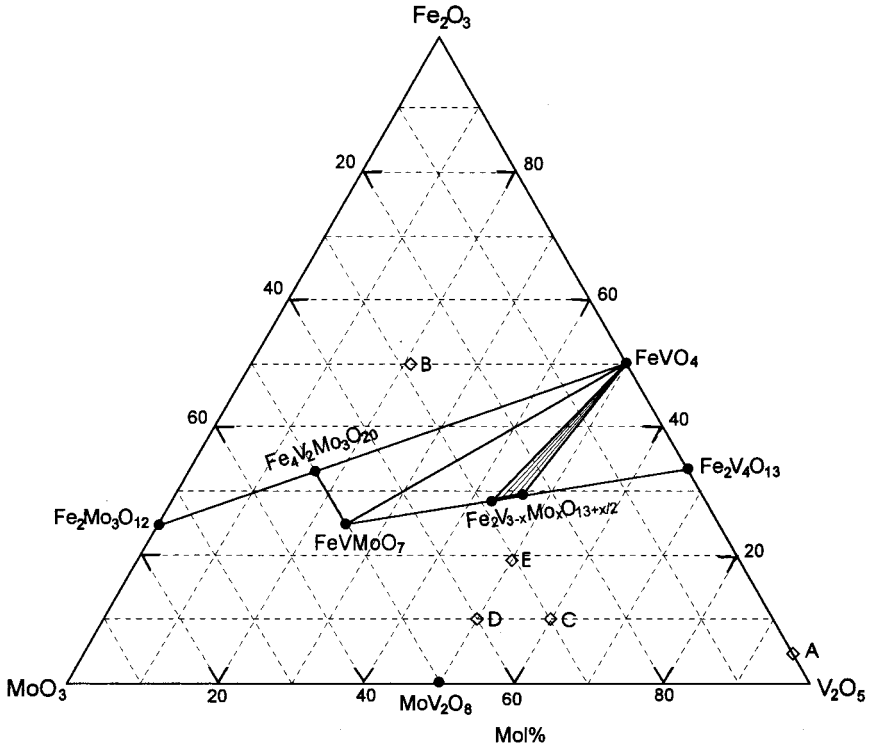

Figure 1. $Fe_2O_3-V_2O_5-MoO_3$ system showing the known compounds and the compositions used for the crystal growth of $Fe_2V_4O_{13}$ and $Fe_2V_{3-x}Mo_xO_{13+x/2}$ ($0.84 \leq x \leq 1.00$).

finally cooled to 40 °C at 60 °C h^{-1}. In the solidified melt, the major crystalline phase was V_2O_5 and the minor phase was the brittle amber/brown crystals of the desired product $Fe_2V_4O_{13}$. In addition, a few small dark crystals of $FeVO_4$ were formed. The two iron vanadate crystals could be separated easily from the vanadium oxide matrix by the difference in hardness. $Fe_2V_4O_{13}$ could usually be distinguished from $FeVO_4$ by color but not always. More crystals used for IR and Raman studies were obtained by simply repeating the above experiment.

$Fe_2V_{3.16}Mo_{0.84}O_{13.42}$ crystals were also grown by a flux method but by two different routes. Route I: Crystals used for study by single-crystal X-ray diffraction were grown using the composition 50 mol % Fe_2O_3 (99.9%, Aldrich), 21.58 mol % V_2O_5 (99.6+%, Aldrich) and 28.42 mol % MoO_3 (99.5%, Aldrich) (composition B in Figure 1). A total of 7.943 g of mixed powder was packed into a platinum crucible covered by an Al_2O_3 crucible, heated to 900 °C at 120 °C h^{-1}, soaked for 2 h, and then cooled to 700 °C at 5 °C h^{-1} and further cooled to room temperature at 60 °C h^{-1}. A total of 1.2% weight loss was observed during the crystal growth. Dark brown platelets were formed, and their approximate compositions were determined by energy dispersive analysis of X-ray (EDAX) to be Fe:V:Mo (atomic ratio) = 2.00:3.2(2):1.1(1). The atomic ratio of V/Mo for the crystals was determined by ICP-AES to be 3.0(1):1.00. The reported composition of the investigated crystal was determined by population refinement on the X-ray diffraction data. Route II: A higher yield of crystals was obtained in a sealed quartz tube using a composition containing more V_2O_5 and MoO_3 than in route I. A mixture of 0.759 g of Fe_2O_3, 5.188 g of V_2O_5, and 2.053 g of MoO_3 (composition C in Figure 1) was ground and sealed in a quartz tube. The sample was heated to 720 °C at 120 °C h^{-1}, soaked for 2 h, then cooled to 520 °C at 4 °C h^{-1} and further cooled to 50 °C at 60 °C h^{-1}. Light yellow thin plates and light brown thick plates were formed. Their average composition was determined by EDAX to be Fe:V:Mo (atomic ratio) = 2.00:3.2(1):1.2(1), consistent with the crystals grown by route I.

Crystals containing more molybdenum, $Fe_2V_{3-x}Mo_xO_{13+x/2}$ ($x > 0.84$), were grown from composition D (see Figure 1). The experimental conditions were identical to those in route II described above. The composition of these crystals was determined by EDAX to be Fe:V:Mo (atomic ratio) = 2.00:3.1(1):1.4(1). Considering the systematic deviation estimated by analyzing the compositions of pure polycrystalline $FeVMoO_7$ and $Fe_4V_2Mo_3O_{20}$ samples, and comparing with the EDAX results on the crystals grown from compositions B and C, we believed that the real composition was very close to $Fe_2V_3MoO_{13.5}$. Finally, solid solution crystals $Fe_2V_{3-x}Mo_xO_{13+x/2}$ ($0.84 \leq x \leq 1.00$) were also grown using composition E (Figure 1).

Crystallographic Determination. Crystals were mounted on glass fibers for study by single-crystal X-ray diffraction on an Enraf-Nonius CAD4 diffractometer. An amber needle ($0.27 \times 0.03 \times 0.03$ mm^3) of $Fe_2V_4O_{13}$ and a dark brown needle ($0.39 \times 0.09 \times 0.06$ mm^3) of $Fe_2V_{3.16}Mo_{0.84}O_{13.42}$ cut from a plate crystal were used for data collection. The observed systematic absences ($h0l$, $l \neq 2n$; $0k0$, $k \neq 2n$) uniquely determine the space group to be $P2_1/c$ for each. The structures were solved by direct methods with SHELXS-86[9] and DIRDIF94[10] and least-squares refined on $|F|$ with TEXSAN.[11] To ensure the correctness of the determined unit cell for $Fe_2V_{3.16}Mo_{0.84}O_{13.42}$, another crystal from the same batch was investigated using a CCD detector. The analyses and results showed no indication of doubling of the unit cell axes. In $Fe_2V_4O_{13}$ metal and oxygen atoms were refined anisotropically and isotropically, respectively. In $Fe_2V_{3.16}Mo_{0.84}O_{13.42}$ all atoms were refined anisotropically. Simultaneous refinements on the partially occupied vanadium, molybdenum, and oxygen sites resulted in the formula $Fe_2V_{3.16}Mo_{0.84}O_{13.50}$, which is consistent with the analyzed composition. In the final refinement, the occupancy of the partially occupied oxygen was fixed for charge balance. Relevant crystallographic information is listed in Table 1 and in more detail in the Supporting Information. Atomic positions and equivalent isotropic thermal parameters are presented in Table 2. Selected bond lengths and angles are listed in Table 3. The standard deviations of the atomic

(9) Sheldrick, G. M. In *Crystallographic Computing 3*; Sheldrick, G. M., Krüger, C., Goddard, R., Eds.; Oxford University Press: London/New York, 1985; pp 175−189.

(10) Beurskens, P. T.; Admiraal, G.; Beurskens, G.; Bosman, W. P.; de Gelder, R.; Israel, R.; Smits, J. M. M. In *The DIRDIF-94 Program System*; Technical Report of the Crystallography Laboratory; University of Nijmegen: The Netherlands, 1994.

(11) (a) TEXSAN: Crystal Structure Analysis Package, Molecular Structure Corp., The Woodlands, TX, 1992. (b) Cromer, D. T.; Waber, J. T. Scattering Factors for Non-hydrogen Atoms. In *International Tables for X-ray Crystallography*; Kynoch Press: Birmingham, England, 1974; Vol. IV, Table 2.2A.

Table 1. Crystallographic Data for $Fe_2V_4O_{13}$ and $Fe_2V_{3.16}Mo_{0.84}O_{13.42}$

empirical formula	$Fe_2V_4O_{13}$	$Fe_2V_{3.16}Mo_{0.84}O_{13.42}$
fw	523.45	567.97
space group	$P2_1/c$ (No. 14)	$P2_1/c$ (No. 14)
a, Å	8.300(2)	7.678(1)
b, Å	9.404(6)	9.456(2)
c, Å	14.560(2)	8.336(2)
β, deg	102.08(1)	109.50(2)
V, Å^3	1111.3(6)	570.5(2)
Z	4	2
T, °C	−120	−120
λ, Å	0.710 69	0.710 69
ρ_{calc}, g/cm^3	3.13	3.31
μ, mm^{-1}	5.83	5.92
R^a	0.041	0.026
$R_w{}^b$	0.038	0.030

^{a} $R = \sum||F_o| - |F_c||/\sum|F_o|$. ^{b} $R_w = [\sum w(|F_o| - |F_c|)^2/\sum w|F_o|^2]^{1/2}$.

Table 2. Positional Parameters and Equivalent Isotropic Displacement Coefficients (Å^2)^a for $Fe_2V_4O_{13}$ and $Fe_2V_{3.16}Mo_{0.84}O_{13.42}$

atom	x	y	z	U(eq)
		$Fe_2V_4O_{13}$		
Fe(1)	0.1893(2)	0.5012(2)	0.0069(1)	0.0042(4)
Fe(2)	0.3081(2)	0.0000(2)	0.98160(9)	0.0039(4)
V(1)	0.5303(2)	0.2123(2)	0.5956(1)	0.0042(5)
V(2)	0.7476(2)	0.2221(2)	0.8278(1)	0.0038(5)
V(3)	0.1438(2)	0.2408(2)	0.8222(1)	0.0024(5)
V(4)	0.9575(2)	−0.2074(2)	0.9081(1)	0.0035(5)
O(1)	0.3498(8)	0.6151(8)	0.9569(5)	0.007(2)
O(2)	0.2305(9)	0.6165(9)	0.1256(5)	0.009(2)
O(3)	0.3460(8)	0.3608(8)	0.0765(5)	0.005(2)
O(4)	0.0082(8)	0.3824(8)	0.0462(5)	0.004(2)
O(5)	0.1615(9)	0.3839(8)	0.8908(5)	0.007(2)
O(6)	0.2858(8)	0.1200(8)	0.8684(5)	0.004(2)
O(7)	0.5055(8)	0.1130(8)	0.0476(5)	0.004(2)
O(8)	0.3151(9)	−0.1127(9)	0.0988(5)	0.011(2)
O(9)	0.1413(8)	−0.1352(8)	0.9094(5)	0.007(2)
O(10)	0.1634(7)	0.2929(8)	0.7075(4)	0.003(1)
O(11)	0.9449(9)	0.1650(7)	0.8122(5)	0.008(2)
O(12)	0.6095(8)	0.2233(8)	0.7178(5)	0.009(2)
O(13)	0.8632(8)	−0.1166(8)	0.9780(5)	0.003(2)
		$Fe_2V_{3.16}Mo_{0.84}O_{13.42}$		
Fe	0.4768(1)	0.5008(1)	0.1787(1)	0.0075(1)
V(1)^b	0.8480(1)	0.7216(1)	0.4246(1)	0.0054(2)
V(2)	1.3179(1)	0.7102(1)	0.4464(1)	0.0061(1)
Mo^c	0.8484(1)	0.7609(1)	0.3175(1)	0.0096(2)
O(1)^d	0.857(1)	0.8346(4)	0.127(1)	0.018(1)
O(2)	1.0825(4)	0.7173(3)	0.4316(4)	0.020(1)
O(3)	0.7078(3)	0.6137(3)	0.2731(3)	0.014(1)
O(4)	0.5614(3)	0.3844(3)	0.3857(3)	0.013(1)
O(5)	0.2454(3)	0.3880(3)	0.0934(3)	0.013(1)
O(6)	0.3385(3)	0.6385(3)	0.2718(3)	0.011(1)
O(7)	0.4092(3)	0.6168(3)	−0.0379(3)	0.009(1)

^{a} U(eq) is defined as one-third of the trace of the orthogonalized $\mathbf{U}_{ij}$ tensor. ^{b} Occupancy = 0.581(2). ^{c} Occupancy = 0.419(2). ^{d} Occupancy = 0.710.

coordinates and bond lengths for $Fe_2V_4O_{13}$ (Tables 2 and 3) are at least four times smaller than those reported for the powder refinement.[6a]

Property Measurement. Raman and infrared spectroscopy were used to characterize the metal−oxygen vibrations of the title compounds. About 100 $Fe_2V_4O_{13}$ crystals and 60 $Fe_2V_3MoO_{13.5}$ crystals were cleaned with ethanol and acetone prior to drying and powdering. All $Fe_2V_4O_{13}$ crystals were checked individually by EDAX (Hitachi S-4500). Mid-infrared (400−4400 cm^{-1}) spectra were collected using a Bio-Rad FTS-60 FTIR spectrophotometer at 2 cm^{-1} resolution. Raman (100−1200 cm^{-1}) spectra were collected on a Bio-Rad FT-Raman spectrophotometer with 4 cm^{-1} resolution (500 scans for $Fe_2V_4O_{13}$, 200 scans for $Fe_2V_{3.16}Mo_{0.84}O_{13.42}$). The purity of the powdered crystals was examined by powder X-ray diffraction on a Rigaku machine (Cu Kα radiation). The melting points of $Fe_2V_4O_{13}$ and $Fe_2V_{3.16}Mo_{0.84}O_{13.42}$ in static air were determined to be 669(2) and 732(2) °C by differential thermal analysis (TA Instruments DSC 2910).

Results and Discussion

Synthesis. Attempts to prepare pure phases of $Fe_2V_4O_{13}$ and $Fe_2V_3MoO_{13.5}$ by solid-state reaction were never successful even though a sealed-tube technique was used in association with multiple steps of grinding and heating. The preparation of $Fe_2V_4O_{13}$ at 640 °C resulted in a mixture of $Fe_2V_4O_{13}$ and $FeVO_4$, and the preparation of $Fe_2V_3MoO_{13.5}$ at 680 °C gave rise to a mixture of $Fe_2V_3MoO_{13.5}$, $FeVO_4$, and $FeVMoO_7$. The sample of $Fe_2V_4O_{13}$ prepared by Permer and Laligant[6a] for refinement of the structure was a mixture of $Fe_2V_4O_{13}$ and $FeVO_4$. The difficulty in preparing a pure $Fe_2V_4O_{13}$ phase is likely due to the sluggish reaction between V_2O_5 and the quickly formed $FeVO_4$ at temperatures where significant evaporation of vanadium species does not occur. Similarly, when the more stable phases $FeVO_4$ and $FeVMoO_7$ are formed, it is difficult for them to react completely with the remaining V_2O_5 to form pure $Fe_2V_3MoO_{13.5}$. This situation is also encountered in the preparation of $MgMo_2O_7$ from MgO and MoO_3,[12] and in the preparation of $Mn_3V_2O_8$ from MnO and V_2O_5.[13] The more stable compounds were $MgMoO_4$ and $Mn_2V_2O_7$, respectively. Under such circumstances it is more feasible to grow single crystals off stoichiometry than to prepare the single phase from the corresponding stoichiometric composition.

Structure. The structure of $Fe_2V_4O_{13}$ is built up from isolated edge-shared Fe_2O_{10} octahedral dimers and *U*-shaped tetrapolyvanadate $V_4O_{13}{}^{6-}$ anions (four corner-shared tetrahedra) (Figure 2) and is isostructural with $Cr_2P_4O_{13}$.[14] The FeO_6 octahedral planes perpendicular to the *c* axis consist of Fe_2O_{10} dimer rows running along the *a* axis. The dihedral angle formed between two adjacent octahedral rows (viewed along the edge-shared oxygen planes) is about 115°. Fe_2O_{10} octahedral dimers are linked with $V_4O_{13}{}^{6-}$ anions through corner-sharing, as shown in Figure 3. $V(2)O_4$ and $V(3)O_4$ tetrahedra are linked to the FeO_6 octahedra (Figure 3a) in a different way from $V(1)O_4$ and $V(4)O_4$ tetrahedra (Figure 3b). Only $V(1)O_4$ and $V(4)O_4$ are linked to the oxygens shared by two Fe^{3+} ions.

One of the remarkable features of the $Fe_2V_4O_{13}$ structure is the rare *U*-shaped $V_4O_{13}{}^{6-}$ anion. To our knowledge, barium vanadate $Ba_3V_4O_{13}$ is the only reported vanadate with a similar $V_4O_{13}{}^{6-}$ motif.[15]

On the basis of a survey of the literature, $V^{5+}O_4$ tetrahedra can also exist as isolated $VO_4{}^{3-}$ anions,[16] divanadate $V_2O_7{}^{4-}$ anions (two tetrahedra are linked by one O(br)),[17] trivanadate $V_3O_{10}{}^{5-}$ anions (three tetrahedra are linked by two O(br)),[18] and infinite zigzag chains $V_nO_{3n+1}{}^{(n+2)-}$ ($n \rightarrow \infty$).[19] The long and short V−O bonds and the estimated tetrahedral distortions for a number of homologous vanadate anions are summarized and compared in Table 4. The V−O(br) bonds are always about 0.1 Å longer than the V−O(nbr) (nonbridging oxygen) bonds. This means that V−O(br) bonds are weaker than V−O(nbr) bonds. In other words V−O(br) bonds are more active than V−O(nbr) bonds under reduction conditions as observed in the

(12) Stadnicka, K.; Haber, J.; Kozlowski, R. *Acta Crystallogr.* **1977**, *B33*, 3859−3862.
(13) (a) Clark, G. M.; Morley, R.; Pick, A. N. *J. Inorg. Nucl. Chem.* **1977**, *39*, 1841−1843. (b) Wang, X. D.; Liu, Z. Q.; Poeppelmeier, K. R.; Dravid, V. P. In preparation.
(14) Lii, K. H.; Chen, Y. B.; Su, C. C.; Wang, S. L. *J. Solid State Chem.* **1989**, *82*, 156−160.
(15) Gatehouse, B. M.; Guddat, L. W.; Roth, R. S. *J. Solid State Chem.* **1987**, *71*, 390−395.

Table 3. Selected Bond Lengths (Å) and Angles (deg) for $Fe_2V_4O_{13}$ and $Fe_2V_{3.16}Mo_{0.84}O_{13.42}$

bond lengths				bond angles	
		$Fe_2V_4O_{13}$			
Fe(1)−O(1)	1.964(7)	Fe(2)−O(6)	1.974(7)	O(1)−V(1)−O(3)	108.6(4)
Fe(1)−O(2)	2.009(8)	Fe(2)−O(7)	2.020(7)	O(1)−V(1)−O(12)	111.4(3)
Fe(1)−O(3)	1.977(7)	Fe(2)−O(7)	1.995(7)	O(3)−V(1)−O(12)	109.4(3)
Fe(1)−O(4)	2.049(7)	Fe(2)−O(8)	1.999(8)	O(1)−V(1)−O(7)	111.1(4)
Fe(1)−O(4)	1.989(7)	Fe(2)−O(9)	2.007(8)	O(3)−V(1)−O(7)	107.0(3)
Fe(1)−O(5)	1.990(7)	Fe(2)−O(13)	1.979(7)	O(7)−V(1)−O(12)	109.2(3)
V(1)−O(1)	1.652(7)	V(3)−O(5)	1.664(8)	V(1)−O(12)−V(2)	161.6(4)
V(1)−O(3)	1.646(7)	V(3)−O(6)	1.673(7)	V(2)−O(11)−V(3)	137.0(4)
V(1)−O(7)	1.780(8)	V(3)−O(10)	1.781(6)	V(3)−O(10)−V(4)	138.3(4)
V(1)−O(12)	1.766(7)	V(3)−O(11)	1.776(7)		
V(2)−O(2)	1.657(8)	V(4)−O(4)	1.775(8)		
V(2)−O(8)	1.646(8)	V(4)−O(9)	1.667(7)		
V(2)−O(11)	1.782(7)	V(4)−O(10)	1.770(6)		
V(2)−O(12)	1.763(7)	V(4)−O(13)	1.646(7)		
		$Fe_2V_{3.16}Mo_{0.84}O_{13.42}$			
Fe(1)−O(3)	1.993(3)	V(2)−O(2)	1.771(3)	O(1)−V(1)−O(2)	104.4(2)
Fe(1)−O(4)	1.965(3)	V(2)−O(4)	1.659(3)	O(1)−V(1)−O(3)	110.2(2)
Fe(1)−O(5)	1.989(3)	V(2)−O(6)	1.661(2)	O(1)−V(1)−O(5)	104.1(2)
Fe(1)−O(6)	1.994(2)	V(2)−O(7)	1.768(3)	O(2)−V(1)−O(3)	113.1(1)
Fe(1)−O(7)	2.026(2)	Mo−O(1)	1.758(4)	O(2)−V(1)−O(5)	114.3(1)
Fe(1)−O(7)	2.016(2)	Mo−O(2)	1.779(3)	O(3)−V(1)−O(5)	110.1(1)
V(1)−O(1)	1.745(4)	Mo−O(3)	1.724(3)	V(1)−O(2)−V(2)	177.8(2)
V(1)−O(2)	1.783(3)	Mo−O(5)	1.694(3)	Mo−O(1)−V(1)	137.4(2)
V(1)−O(3)	1.699(3)			Mo−O(2)−V(2)	150.7(2)
V(1)−O(5)	1.715(3)				

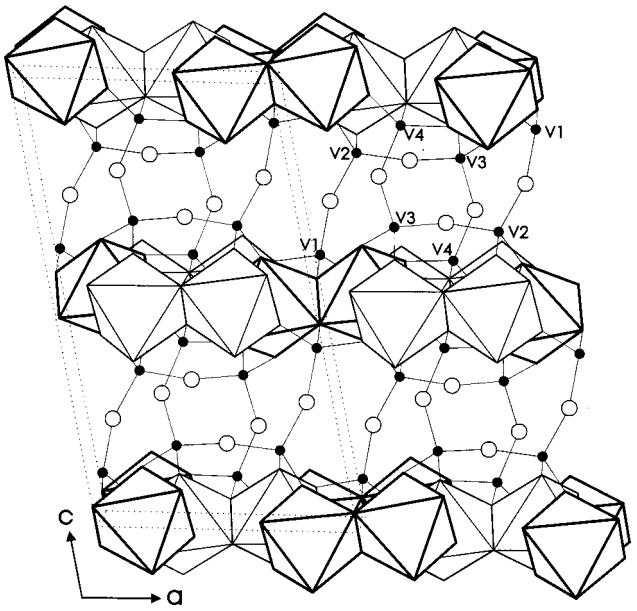

Figure 2. Structure of $Fe_2V_4O_{13}$ viewed approximately along the *b* axis: $Fe(1)O_6$ octahedra, dark lines; $Fe(2)O_6$ octahedra, normal lines; V, shaded balls; bridging O, circles; unit cell, dotted lines.

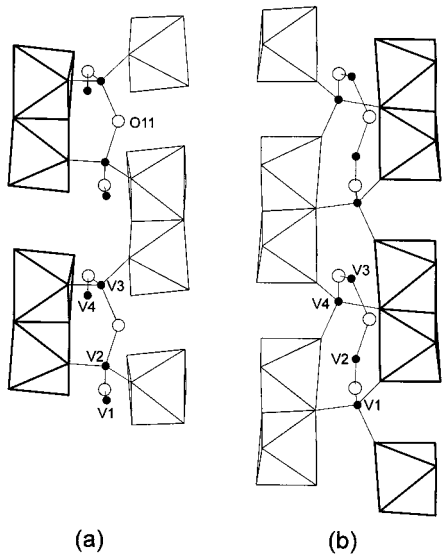

Figure 3. Linkage between Fe_2O_{10} octahedral dimers and $V_4O_{13}^{6-}$ clusters approximately along the *c* axis in $Fe_2V_4O_{13}$: (a) between two intermediate $V(2)O_4$ and $V(3)O_4$ tetrahedra and FeO_6 octahedra; (b) between terminal $V(1)O_4$ and $V(4)O_4$ tetrahedra and FeO_6 octahedra.

pyrovanadate $Mg_2V_2O_7$ catalyst tested for the dehydrogenation of propane.[1a,c] The estimated tetrahedral distortion parameters for $Fe_2V_4O_{13}$ (1.09−1.36) are relatively smaller than those of other polyanions $V_nO_{3n+1}^{(n+2)-}$ ($n \geq 2$) (Table 4).

The structure of $Fe_2V_{3.16}Mo_{0.84}O_{13.42}$ is built up from isolated edge-shared Fe_2O_{10} octahedral dimers and disordered *U*-shaped polyvanadomolybdate $[V_{3.16}Mo_{0.84}O_{13.42}]^{6-}$ anions (Figure 4). The disorder is displayed in the partially occupied V(1), Mo,

(16) Vanadates containing isolated VO_4 tetrahedra have been described. In cation-deficient spinels, (a) $Mg_3V_2O_8$: Krishnamachari, N.; Calvo, C. *Can. J. Chem.* **1971**, *49*, 1629−1637. (b) $Co_3V_2O_8$, $Ni_3V_2O_8$: Sauerbrei, E. E.; Faggiani, R.; Calvo, C. *Acta Crystallogr.* **1973**, *B29*, 2304−2305. (c) α-$Zn_3V_2O_8$: Gopal, R.; Calvo, C. *Can. J. Chem.* **1971**, *49*, 3056−3059. (d) $Mn_3V_2O_8$: ref 13b. In $CrVO_4$-type structures, (e) $CrVO_4$: Frazer, B. C.; Brown, P. J. *Phys. Rev.* **1962**, *125*, 1283−1291. (f) $FeVO_4$-II: Oka, Y.; Yao, T.; Yamamoto, N.; Ueda, Y.; Kawasaki, S.; Azuma, M.; Takano, M. *J. Solid State Chem.* **1996**, *123*, 54−59. (g) $InVO_4$: Touboul, M.; Toledano, P. *Acta Crystallogr.* **1980**, *B36*, 240−245. In zircon-type structures, (h) MVO_4 (M = Sc, Y, Ce, Pr, Nd, Tb, Ho, Er, Tm, Yb, Lu): Chakoumakos, B. C.; Abraham, M. M.; Boatner, L. A. *J. Solid State Chem.* **1994**, *109*, 197−202.

(17) Vanadates containing $V_2O_7^{3-}$ anions have been described. (a) $Co_2V_2O_7$, $Ni_2V_2O_7$: Sauerbrei, E. E.; Faggiani, R.; Calvo, C. *Acta Crystallogr.* **1974**, *B30*, 2907−2909. (b) $Cs_3Mn_3V_4O_{16}$: Le Page, Y.; Strobel, P. *Inorg. Chem.* **1982**, *21*, 620−623. (c) $Ba_2V_2O_7$: Hawthorne, F. C.; Calvo, C. *J. Solid State Chem.* **1978**, *26*, 345−355.

(18) Kato, K.; Takayama-Muromachi, E. *Acta Crystallogr.* **1985**, *C41*, 647−649.

(19) (a) Liao, J. H.; Sigala, C.; Guyomard, D.; Piffard, Y. *Acta Crystallogr.* **1996**, *C52*, 283−284. (b) Tabuteau, A.; Cousson, A.; Pages, M. *Acta Crystallogr.* **1979**, *B35*, 2000−2002.

Table 4. Comparison of Average V−O Bond Lengths (Å) and Tetrahedral Distortion[a] ($\Delta \times 10^3$) Ranges for $V_nO_{3n+1}^{(n+2)-}$ Anions Formed through Corner-Shared VO_4 Tetrahedra

polyanion	*n*	compd	V−O(br)[b]	V−O(nbr)[c]	($\Delta \times 10^3$)	ref
VO_4^{3-}	1	$Mg_3V_2O_8$		1.729	0.74	16a
		$FeVO_4$-II		1.722	1.65	16f
$V_2O_7^{4-}$	2	$Co_2V_2O_7$	1.849	1.694	1.31−2.01	17a
		$Cs_3Mn_3V_4O_{16}$	1.811	1.698	1.35−1.91	17b
$V_3O_{10}^{5-}$	3	$K_5V_3O_{10}$	1.788	1.648	1.48−2.02	18
$V_4O_{13}^{6-}$	4	$Ba_3V_4O_{13}$	1.798	1.667	1.32−1.57	15
		$Fe_2V_4O_{13}$	1.773	1.681	1.09−1.36	this work
$V_nO_{3n+1}^{(n+2)-}$	∞	$K_2Mn(VO_3)_4$	1.789	1.641	1.29−2.36	19a
		$Np(VO_3)_4$	1.766	1.641	1.11−1.95	19b

[a] $\Delta = {}^1/_4\sum[(R_i - R)/R]^2$, where R_i and R are the individual and average bond lengths for each tetrahedron. [b] Bridging oxygens. [c] Nonbridging oxygens.

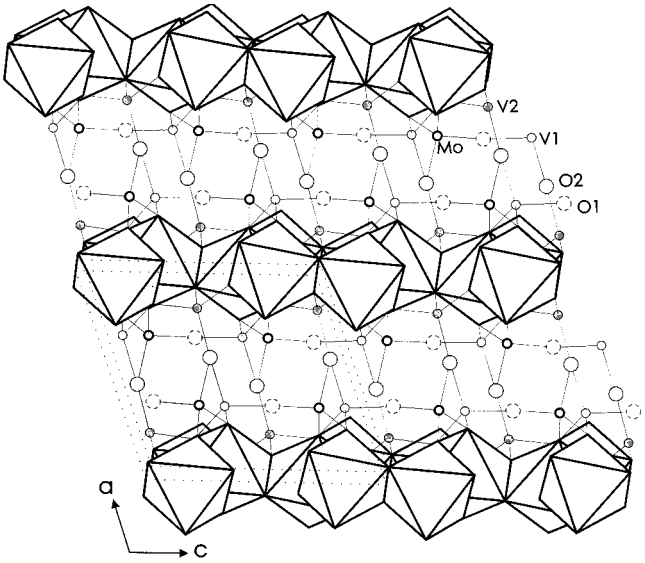

Figure 4. Structure of $Fe_2V_{3.16}Mo_{0.84}O_{13.42}$ viewed approximately along the *b* axis: FeO_6 octahedra, dark lines; other atoms, labeled; unit cell, dotted lines.

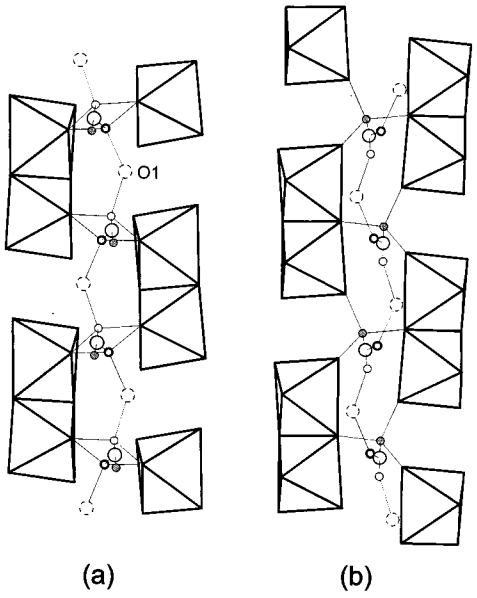

Figure 5. Linkages between Fe_2O_{10} octahedral dimers and $[V_{3.16}Mo_{0.84}O_{13.42}]^{6-}$ clusters approximately along the *a* axis in $Fe_2V_{3.16}Mo_{0.84}O_{13.42}$: (a) between Fe_2O_{10} dimers and nonterminal tetrahedra ($V(1)O_4$ and MoO_4); (b) between Fe_2O_{10} dimers and terminal $V(2)O_4$ tetrahedra. The labels for atoms are the same as in Figure 4.

and O(1) sites, whose occupancies are 0.58, 0.42, and 0.71, respectively (Table 2). The least squares refinement on seven possible models of the order/disorder of V and Mo on the two face-shared tetrahedral sites shows no site mixing between V and Mo atoms. Bond valence calculations (Mo = +6.3, V = +4.8)[20] agree with the refined results. The face-shared tetrahedral coordination probably should not be considered as trigonal bipyramidal coordination because both the V(1) and Mo atoms are centered in the tetrahedra. The distance between a V(1) or Mo atom and O(1) is about 1.75 Å (see Table 3) whereas the distance is almost 2.71 Å to the opposite oxygen atom in the face-shared configuration. The arrangement of Fe_2O_{10} dimers in space is essentially the same as in $Fe_2V_4O_{13}$. The dihedral angle between two adjacent octahedral rows is about 113°, similar to the equivalent angle (115°) in $Fe_2V_4O_{13}$. The estimated $V(1)O_4$ and $V(2)O_4$ tetrahedral distortions ($\Delta \times 10^3$) are 0.34 and 1.02, respectively. This indicates that the distortion of $V(1)O_4$ is smaller than that of any of the VO_4 tetrahedra listed in Table 4. The distortion of the MoO_4 tetrahedra is also very small ($\Delta \times 10^3 = 0.35$). Fe_2O_{10} dimers are linked together by the disordered *U*-shaped $[V_{3.16}Mo_{0.84}O_{13.42}]^{6-}$ anions (Figure 5). Again, the connection of $V(1)O_4$ and MoO_4 to FeO_6 is different from the connection of $V(2)O_4$ to FeO_6. However, the linkage of the two nonterminal tetrahedra to FeO_6 (Figure 5a) is very similar to that (Figure 3a) in $Fe_2V_4O_{13}$, and the linkage of the two terminal tetrahedra to FeO_6 (Figure 5b) is also similar to that (Figure 3b) in $Fe_2V_4O_{13}$. The middle bridging oxygen O(1) distributes equivalently on both sides between the two adjacent FeO_6 octahedral rows, which is apparently different from the O(11) in $Fe_2V_4O_{13}$ (Figure 3). It appears that the O(1) position is equivalent to the sum of the O(11) position and the vacancy between two adjacent $V_4O_{13}^{6-}$ anions (see Figure 3).

Structural Comparison of $Fe_2V_4O_{13}$ and $Fe_2V_{3.16}Mo_{0.84}O_{13.42}$ with $FeVMoO_7$. As described above on the basis of polyhedra and their connectivity, the two structures of the title compounds are very similar except for the disorder of the middle bridging oxygen and the splitting of the nonterminal tetrahedral sites in the latter. All tetrahedra are relatively regular as illustrated by giving the bond angles (Table 3) for one of the tetrahedra (V(1)) in each compound. However, if we compare the Newman-type projections (Figure 6) looking along every neighboring metal−metal axis to show the oxygen atoms for the *U*-shaped polyanions, we will find that all three double tetrahedra twist counterclockwise in $Fe_2V_4O_{13}$ (Figure 6a) and twist clockwise in $Fe_2V_{3.16}Mo_{0.84}O_{13.42}$ (Figure 6b). This surprising difference in stereoconfiguration provides us a better understanding of the two different structures. The average twist angles are 15.4° (V1−V2), 52.1° (V4−V3), and 14.1° (V2−V3) for $Fe_2V_4O_{13}$

(20) Brown, I. D.; Altermatt, D. *Acta Crystallogr.* **1985**, *B41*, 244−247.
(21) Shannon, R. D. *Acta Crystallogr.* **1976**, *A32*, 751−767.

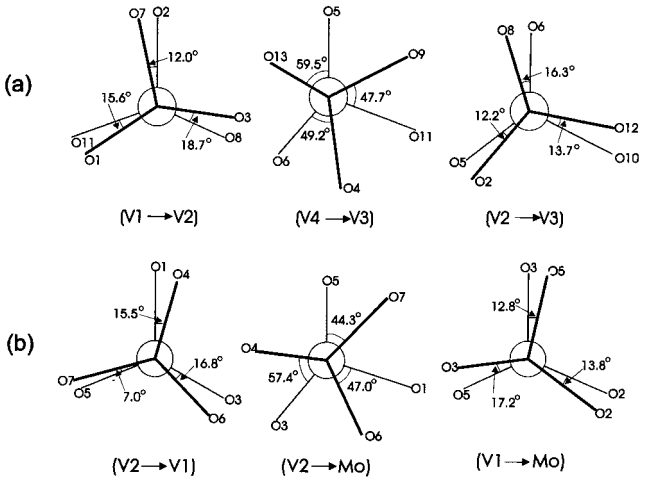

Figure 6. Newman projections: (a) down V1−V2, V4−V3 and V2−V3 in $Fe_2V_4O_{13}$; (b) down V2−V1, V2−Mo, and V1−Mo in $Fe_2V_{3.16}Mo_{0.84}O_{13.42}$.

Table 5. Comparison of Some Structural Parameters and Estimated FeO_6 Distortion Δ[a] for $Fe_2V_4O_{13}$, $Fe_2V_{3.16}Mo_{0.84}O_{13.42}$, and $FeVMoO_7$

formula	Z	d_x (g/cm^3)	FeO_6-FeO_6[b] (Å)	Fe−O[c] (Å)	$\Delta \times 10^4$
$Fe_2V_4O_{13}$	4	3.13	7.280(1)	1.996(7)	1.24
$Fe_2V_{3.16}Mo_{0.84}O_{13.42}$	2	3.31	7.678(1)	1.997(3)	0.97
$FeVMoO_7$	2	3.66	7.909(1)	1.992(3)	2.03

[a] $\Delta = {}^1/_6\sum[(R_i - R)/R]^2$, where R_i and R are the individual and average bond lengths, respectively.[21] [b] Distances between FeO_6 planes. [c] Average Fe−O bond distance.

and 13.1° (V2−V1), 49.6° (V2−Mo), and 14.6° (V1−Mo) for $Fe_2V_{3.16}Mo_{0.84}O_{13.42}$, which indicates that the polyanions resemble eclipsed and staggered conformations.

$Fe_2V_4O_{13}$, $Fe_2V_{3.16}Mo_{0.84}O_{13.42}$, and $FeVMoO_7$ reside on the same line in the $Fe_2O_3-V_2O_5-MoO_3$ system (Figure 1), indicating that their compositions follow the substitution regime of Mo^{6+} for V^{5+}. Each structure contains isolated Fe_2O_{10} octahedral dimers that are aligned in the same direction in space, but in the first two structures the dimers form planes either parallel to the *ab* plane (Figure 2) or parallel to the *bc* plane (Figure 4), while in the third structure they form zigzag planes between which $[VMoO_7]^{3-}$ anions are located.[7a] The distance between two adjacent planes and the crystal density increase with the molybdenum content (Table 5), which reflects the difference in the effective ionic radii and atomic masses of Mo^{6+} and V^{5+}. The average Fe−O bond lengths in the three structures are almost identical, but $FeVMoO_7$ has a larger octahedral distortion value than the other two species.

The evolution of the arrangements of MO_4 tetrahedra in the structures can be best illustrated and compared in Figure 7. Comparing $[V_{3.16}Mo_{0.84}O_{13.42}]^{6-}$ with $V_4O_{13}^{6-}$, it can be regarded that the substitution of Mo^{6+} for V^{5+} only takes place on the two nonterminal tetrahedral sites, which results in the splitting of the tetrahedral sites and disordering of the bridging oxygen atoms with the extra introduced oxygen (Figure 7a,b). Only one of the two face-shared tetrahedra is actually occupied by either VO_4 or MoO_4. Locally, the disordered $Fe_2V_{3.16}Mo_{0.84}O_{13.42}$ could contain regular *U*-shaped units $[V_3MoO_{13}]^{5-}$, tetrahedral dimers $[VMoO_7]^{3-}$ forming Mo═O oxo double bonds and tetrahedral dimers $V_2O_7^{4-}$ forming V═O oxo double bonds (Figure 7b). On the basis of the fact that Mo═O oxo double bonds are formed in $FeVMoO_7$[7a] and

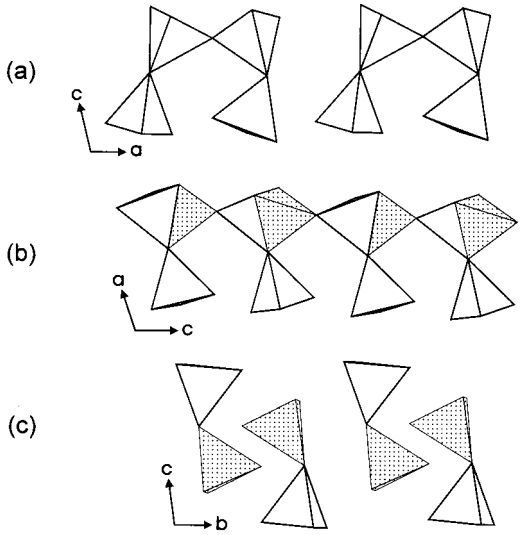

Figure 7. Comparison of the tetrahedral clusters: (a) $V_4O_{13}^{6-}$ in $Fe_2V_4O_{13}$; (b) $[V_{3.16}Mo_{0.84}O_{13.42}]^{6-}$ in $Fe_2V_{3.16}Mo_{0.84}O_{13.42}$; (c) $[VMoO_7]^{3-}$ in $FeVMoO_7$.

Mo^{6+} has a higher valence than V^{5+}, the metal−oxo double bonds in $Fe_2V_{3.16}Mo_{0.84}O_{13.42}$ are more likely to be Mo═O than V═O. If we assume that the nonterminal tetrahedra in the disordered *U*-shaped units are purely occupied by MoO_4, this will result in tetrahedral dimers $[VMoO_7]^{3-}$ in which all the Mo═O oxo double bonds point in approximately the same direction. It can be imagined that such a configuration will not be stable and in some fashion dimers form as observed in $FeVMoO_7$ (Figure 7c).

Substitution Mechanism of Mo^{6+} for V^{5+}. The substitution mechanism of Mo^{6+} for V^{5+} should be described by the formula $Fe_2V_{4-x}Mo_xO_{13+x/2}$ ($0 \le x \le 1$) (not a complete solid solution) rather than the formula $Fe_2V_{4-x}Mo_xO_{13}$ ($0 \le x \le 1$), indicating that the substitution causes no reduction of either V^{5+} or Mo^{6+} ions. The overall charge is balanced by the introduced oxygen atoms accompanying the substitution of Mo^{6+} for V^{5+}. This mechanism is different from that observed in the solid solutions $M_{2.5+x}V_{1+2x}Mo_{1-2x}O_8$ (M = Mg^{2+}, Zn^{2+}, and Mn^{2+}),[4] in which the charge is balanced by changing the fraction of M^{2+} cation vacancies. Also, in the latter case V^{5+} and Mo^{6+} are completely disordered and in the former case they are ordered to a large extent. Common to both mechanisms it is observed that both vanadium and molybdenum preserve their highest oxidation states, which is very different from the partial reduction[22] of Mo^{6+} to Mo^{5+} and V^{5+} to V^{4+} in the well-known $V_{2-x}Mo_xO_5$ ($0 \le x \le 0.3$) ($x \le 0.2$, orthorhombic; $x = 0.3$, monoclinic) solid solution.[22,23] For the substitution of V^{5+} for Mo^{6+} in $K_xV_xMo_{1-x}O_3$ ($x \le 0.13$), although vanadium and molybdenum preserve their highest oxidation states, the charge is balanced by the inserted potassium ions.[24] In all other vanadomolybdates the substitution between V^{5+} and Mo^{6+} causes no change in oxygen content in their structures, which makes the present substitution mechanism unique. It was noted in sol−gel prepared $Fe_{0.12}V_2O_{5.15}$[25] that an extra 0.15 oxygen had been introduced into the V_2O_5 structure accompanying the insertion of Fe^{3+} ions

(22) Bielanski, A.; Najbar, M. *Appl. Catal.* **1997**, *A157*, 223−261.
(23) Kihlborg, L. *Acta Chem. Scand.* **1967**, *21*, 2495−2502.
(24) Darriet, B.; Galy, J. *J. Solid State Chem.* **1973**, *8*, 189−194.
(25) Maingot, S.; Deniard, Ph.; Baffier, N.; Pereira-Ramos, J. P.; Kahn-Harari, A.; Brec, R. In *Soft Chemistry Routes to New Materials*; Rouxel, J., Tournoux, M., Brec, R., Eds.; Materials Science Forum Vols. 152−153; Trans Tech Publications: Switzerland, 1994; pp 297−304.

Table 6. Raman Bands (cm^{-1}) and IR Absorptions (cm^{-1}) for $Fe_2V_4O_{13}$ (A) and $Fe_2V_{3.16}Mo_{0.84}O_{13.42}$ (B)

Raman[a]		IR[a]	
A	B	A	B
971 s	966 s	979 m br	971 m br
938 m br	938 m br	949 m	943 s
909 m br	907 m br	935 m	
859 s	858 s	873 m br	880 m br
822 m	823 m	832 s br	840 m br
793 s	784 s br	796 w	788 w
751 m	747 w br	774 w	
695 m	697 m	710 s	684 s
492 w	492 w br	677 m	
425 m	420 m	621 s	636 m br
382 w br	383 w	581 w sh	575 w sh
348 w br	346 w	526 m	514 w
282 w	275 w sh	477 s	475 s
268 m	262 w		
170 m	170 m		

[a] s = strong, m = moderate, w = weak; b = broad, sh = shoulder.

causing essentially no reduction of V^{5+}, but the extra oxygen has not been well characterized. The different substitution mechanisms of molybdenum for vanadium (or vice versa) are probably determined by the parent structures, but oxygen partial pressure and reaction temperature are also two factors affecting the substitution mechanism.

Properties. The Raman shifts and IR absorptions of $Fe_2V_4O_{13}$ and $Fe_2V_{3.16}Mo_{0.84}O_{13.42}$ on powdered single-crystal samples are summarized in Table 6. The former contains a very small amount ($\leq$5%) of $FeVO_4$, and the latter is phase pure by XRD (Figure 8). The Raman shifts below 600 cm^{-1} of these two compounds are almost identical and very similar to those of $FeVMoO_7$.[7a] These Raman shifts are assigned to the Fe_2O_{10} octahedral dimers. Above 600 cm^{-1}, the Raman shifts are also very similar but quite different from those of $FeVMoO_7$. It is difficult to tell any differences in vibrations between $V_4O_{13}^{6-}$ and $[V_{3.16}Mo_{0.84}O_{13.42}]^{6-}$ anions from Raman study. Most of the IR absorptions are similar between the two compounds (Table 6). However, two IR absorptions, 949 and 935 cm^{-1}, in $Fe_2V_4O_{13}$ changed into one absorption, 943 cm^{-1}, in $Fe_2V_{3.16}Mo_{0.84}O_{13.42}$. Similarly, absorptions 796 and 774 cm^{-1} changed into 788 cm^{-1}, and absorptions 710 and 677 cm^{-1} changed into 684 cm^{-1}. The decrease in the number of IR absorptions reflects the change of the local symmetry and disorder of the $[V_{3.16}Mo_{0.84}O_{13.42}]^{6-}$ anions.

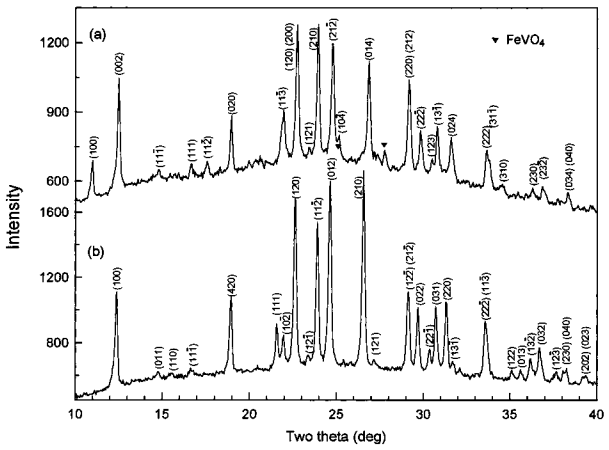

Figure 8. XRD patterns of the powdered crystals: (a) $Fe_2V_4O_{13}$ contaminated with $FeVO_4$, whose two strongest reflections are marked; (b) $Fe_2V_{3.16}Mo_{0.84}O_{13.42}$.

Conclusions

The structures of $Fe_2V_4O_{13}$ and $Fe_2V_{3.16}Mo_{0.84}O_{13.42}$ were determined by single-crystal X-ray diffraction and compared in detail. A new substitution mechanism of Mo^{6+} for V^{5+} in $Fe_2V_{4-x}Mo_xO_{13+x/2}$ ($0 \leq x \leq 1$) has been established, in which the substitution causes no reduction of V^{5+} and Mo^{6+}. Instead, an appropriate amount of oxygen is brought into the structure for charge neutrality. This new mechanism is compared with known substitution mechanisms such as in $M_{2.5+x}V_{1+2x}Mo_{1-2x}O_8$ ($M = Mg^{2+}$, Zn^{2+}, and Mn^{2+}) and $V_{2-x}Mo_xO_5$ ($0 \leq x \leq 0.3$). The redox chemistry and surface catalytic properties of the title compounds are worthy of future study.

Acknowledgment. The authors thank Dr. Larry Cirjak and acknowledge an Extramural Research Award (EMRA) from BP America, Inc., the National Science Foundation, Solid State Chemistry (Award No. DMR-9412971 and DMR-9727516), and the use of central facilities supported by the MRSEC program of the National Science Foundation (Grant DMR-9632472) at the Materials Research Center of Northwestern University.

Supporting Information Available: Two X-ray crystallographic files, in CIF format, are available on the Internet only. Access information is given on any current masthead page.

IC980942T